AIP | The Journal of Chemical Physics

Water anomalous thermodynamics, attraction, repulsion, and hydrophobic hydration

Claudio A. Cerdeiriña and Pablo G. Debenedetti

Citation: The Journal of Chemical Physics **144**, 164501 (2016); doi: 10.1063/1.4947062
View online: http://dx.doi.org/10.1063/1.4947062
View Table of Contents: http://scitation.aip.org/content/aip/journal/jcp/144/16?ver=pdfcov
Published by the AIP Publishing

Water anomalous thermodynamics, attraction, repulsion, and hydrophobic hydration

Claudio A. Cerdeiriña[1,a)] and Pablo G. Debenedetti[2,b)]
[1]*Departamento de Física Aplicada, Universidad de Vigo—Campus del Agua, Ourense 32004, Spain*
[2]*Department of Chemical and Biological Engineering, Princeton University, Princeton, New Jersey 08544, USA*

(Received 8 January 2016; accepted 5 April 2016; published online 22 April 2016)

A model composed of van der Waals-like and hydrogen bonding contributions that simulates the low-temperature anomalous thermodynamics of pure water while exhibiting a second, liquid-liquid critical point [P. H. Poole *et al.*, Phys. Rev. Lett. **73**, 1632 (1994)] is extended to dilute solutions of nonionic species. Critical lines emanating from such second critical point are calculated. While one infers that the smallness of the water molecule may be a relevant factor for those critical lines to move towards experimentally accessible regions, attention is mainly focused on the picture our model draws for the hydration thermodynamics of purely hydrophobic and amphiphilic non-electrolyte solutes. We first focus on differentiating solvation at constant volume from the corresponding isobaric process. Both processes provide the same viewpoint for the low solubility of hydrophobic solutes: it originates from the combination of weak solute-solvent attractive interactions and the specific excluded-volume effects associated with the small molecular size of water. However, a sharp distinction is found when exploring the temperature dependence of hydration phenomena since, in contrast to the situation for the constant-V process, the properties of pure water play a crucial role at isobaric conditions. Specifically, the solubility minimum as well as enthalpy and entropy convergence phenomena, exclusively ascribed to isobaric solvation, are closely related to water's density maximum. Furthermore, the behavior of the partial molecular volume and the partial molecular isobaric heat capacity highlights the interplay between water anomalies, attraction, and repulsion. The overall picture presented here is supported by experimental observations, simulations, and previous theoretical results. *Published by AIP Publishing.* [http://dx.doi.org/10.1063/1.4947062]

I. INTRODUCTION

At atmospheric pressure, $p \simeq 1$ atm, the temperature dependence of the density ρ of water is anomalous, with a maximum at $T_{\mathrm{MD}} \simeq 277$ K that implies a negative isobaric thermal expansivity $\alpha_p \equiv -(\partial \ln \rho/\partial T)_p$ for $T < T_{\mathrm{MD}}$. As temperature is lowered down to the deeply supercooled regime, $|\alpha_p|$ increases steeply in a fashion that resembles the behavior of thermodynamic response functions near critical points. The isothermal compressibility $\kappa_T \equiv (\partial \ln \rho/\partial p)_T$ and the isobaric heat capacity $C_p \equiv T(\partial S/\partial T)_p$ —where S stands for the entropy— also exhibit such seemingly pre-diverging behavior. Equally, dynamic properties like the viscosity or the diffusivity show anomalies in the supercooled region.[1,2]

The molecular origins of this behavior are to be found in the special nature of hydrogen bonding in water, which at low temperatures leads to a four-coordinated, tetrahedral structure characterized by local low-density and low-entropy states that are energetically favored.[1–3] These special microscopic features and the concomitant unusual phenomenology are consistent with the existence of a liquid-liquid critical point that, mainly on the basis of molecular simulation[4] and theory,[5] has been hypothesized to exist at low temperatures and high pressures. Associated with such a critical point is the coexistence of two liquid phases of different density: a low-density phase in which tetrahedral order prevails and a high-density disordered one.

This second phase transition is, however, believed to occur in a region, often referred to as the "no man's land," which is very hard to access experimentally. This region is bounded above by the homogeneous nucleation temperature line,[6] below which water cannot exist as a liquid without rapid crystallization. This is, understandably, a major challenge when trying to obtain direct, unambiguous evidence of the existence of the critical point. As a consequence, an experimental proof is being pursued indirectly via studies on water in confining geometries[7] and on dilute aqueous solutions.[8] In both cases, the homogeneous nucleation temperature is significantly lowered, but mixtures are particularly interesting in that, in addition, a second component develops a line of critical points that could eventually shift the second, isolated critical point to experimentally accessible regions.

Water is also special as a solvent. This statement has its roots on the particular features of aqueous solvation of sparingly soluble, nonpolar molecules such as hydrocarbons and noble gases.[9,10] One such feature is the minimum in the solubility of purely hydrophobic solutes as a function of temperature. In addition, the solvation entropy for solutes of varying size has been found to take nearly the same value at a temperature known as the convergence

a)Electronic address: calvarez@uvigo.es
b)Electronic address: pdebene@princeton.edu

temperature. Specifically, entropy convergence as well as its enthalpic counterpart have been experimentally observed for a variety of families of nonpolar solutes[11] while it has been pointed out that proteins also display such phenomena,[11,12] this being one of the reasons why a strong connection between hydrophobicity and protein thermodynamics has been suggested (see, e.g., Ref. 9). Remarkable is also the fact that the solvation heat capacity of nonpolar solutes takes unusually large positive values, a feature that is usually regarded as the first observed manifestation of hydrophobicity (see Ref. 10).

As a microscopic interpretation underlying the anomalous pattern of solvation of small hydrophobes—in contrast to large objects like macromolecules—as early as 1945 Frank and Evans[13] proposed that this class of solutes strengthens hydrogen bonds of water molecules in the hydration shell. The accuracy and validity range of this picture, known as the "iceberg model," have been under debate ever since being formulated.[14] And even accepting the statement that water structure is enhanced around small hydrophobic solutes, it is unlikely that this is the only source of its anomalous behavior as a solvent.

Indeed, it is natural to inquire whether or not the peculiar thermodynamics of water when it acts as a solvent is related to that of the pure liquid. As a relevant result in this connection, with the aid of molecular simulation, Garde *et al.*[15] found that the entropy convergence phenomenon should be a consequence of the density and related anomalies of water. This conclusion was corroborated by Ashbaugh *et al.*[16] and Graziano.[17]

The analysis by Ashbaugh *et al.* stems from a statistical mechanical model of a pure fluid that exhibits "waterlike" properties including a second critical point.[18] Its extension to mixtures serves as a molecular thermodynamic theory of hydrophobic hydration in which, among other results, a clear link between the density maximum and the solubility minimum is established. Such extended model led Chatterjee and Debenedetti to study the critical loci that originate at the liquid-liquid critical point upon the addition of a second component.[8]

Here we revisit these approaches to the behavior of dilute solutions of a waterlike solvent in the framework of an alternative model. We start from early work by Poole *et al.*[5] in which a model free energy for pure water containing van der Waals-like and hydrogen bonding contributions was shown to give rise to a phase diagram that, for an appropriate choice of model parameters, exhibits a liquid-liquid critical point. Such a model, described in detail in Section II, is extended in Section III to nonelectrolyte solutions. This latter section also contains information on the lines emanating from the second critical point.

Section IV shows the implications that our extended Poole *et al.* model draws for the constant-volume solvation process of small solutes. Attention is devoted to the role of excluded-volume effects and solute-solvent attractive interactions on the solubility of both pure hydrophobes and amphiphilic molecules. Analysis of solvation at constant pressure is performed in Section V. Phenomena like the solubility minimum, enthalpy and entropy convergence, and the behavior of the partial molecular volume and the partial molecular heat capacity are found to entail a revealing interplay between the anomalous thermodynamics of water and intermolecular forces, attractive and repulsive. Results are summarized and further discussed in Section VI.

II. POOLE *ET AL.* MODEL

A. van der Waals-like part

Let us consider the Helmholtz free energy per unit volume $f \equiv F/V$ as being composed of van der Waals-like and hydrogen-bonding contributions,

$$f = f_{\mathrm{vdW}} + f_{\mathrm{HB}}. \tag{1}$$

The f_{vdW} part should contain the ever-present translational contribution as well as further terms arising from internal degrees of freedom (rotation, vibration, etc.), the latter of which we ignore in our coarse-grained description. We choose a hard-sphere part given by the Carnahan and Starling equation of state.[19,20] Together with the usual van der Waals term arising from attractive forces, this constitutes the relevant part of f_{vdW}.

We thus start from

$$p_{\mathrm{vdW}} = \rho k_B T\,[1 + h_2(y)] - a\rho^2, \tag{2}$$

where k_B denotes the Boltzmann constant, $\rho \equiv N/V$ is the number density, a the van der Waals parameter accounting for the effect of attractive forces, and $h_2(y) \equiv (4y - 2y^2)/(1 - y)^3$, with $y \equiv b\rho$ the packing fraction that quantifies excluded-volume effects.[21] Now, on the basis of the thermodynamic relation $(\partial F/\partial V)_T = -p$, one integrates $p_{\mathrm{vdW}}(N/V,T) - Nk_BT/V$ with T and N fixed from a general V to $V = +\infty$. In this way one gets the difference between f_{vdW} and its ideal-gas counterpart so that

$$f_{\mathrm{vdW}} = \rho k_B T\left\{\ln[\rho\Lambda^3(T)] + h_1(y) - 1\right\} - a\rho^2, \tag{3}$$

where $h_1(y) \equiv (4y - 3y^2)/(1 - y)^2$,[22] while $\Lambda(T) \equiv h/(2\pi m k_B T)^{\frac{1}{2}}$ is the thermal de Broglie wavelength, with m and h denoting the mass of a water molecule and Planck's constant, respectively.

B. Hydrogen-bonding part

As a rough but reasonable approximation for water in the liquid state, characterized by a three-dimensional network due to hydrogen bonding, Poole *et al.* assumed that every molecule participates in four hydrogen bonds. Hence, f_{HB} in (1) is twice the free energy per bond. Bonds of two types, "strong" and "weak," are considered. Formation of strong bonds requires a specific intermolecular distance but also favorable mutual orientations between molecules. Such bonds are characterized by a lower energy so that $\varepsilon_{\mathrm{HB}} \equiv \varepsilon_{\mathrm{weak}} - \varepsilon_{\mathrm{strong}}$ is defined.

To accommodate this microscopic scheme, let us appeal to a two-fluid description[23] of the thermodynamic behavior of those $2N$ bonds. A fraction g_0 of them, which we label as A, verify intermolecular-distance restrictions so that they are strong whenever orientational constraints are fulfilled, with the remaining ones, a fraction of $1–g_0$ bonds labeled as B, being weak regardless orientation. It is natural to regard g_0 a function of density. Specifically, on considering a typical

distance for hydrogen bonding, an optimal system density ρ_{HB} is defined. This means that for $\rho = \rho_{HB}$ all hydrogen bonds are strong as long as molecules are properly oriented. Following Poole *et al.*, a Gaussian dependence is chosen,[24]

$$g_0(\rho) = \exp\{-[(\rho - \rho_{HB})/\sigma]^2\}, \quad (4)$$

where σ characterizes the width of the Gaussian.

Orientational selectivity is built in by simply assuming that just one of the $\Omega + 1$ (with $\Omega \gg 1$) accessible states of a given bond is strong. The thermal behavior of the $2N$ independent bonds is then described by the individual partition functions $z^A_{HB} = \Omega \exp(-\varepsilon_{weak}/k_BT) + \exp(-\varepsilon_{strong}/k_BT)$ and $z^B_{HB} = (\Omega + 1)\exp(-\varepsilon_{weak}/k_BT)$. As a result,

$$f_{HB} = -2\rho k_B T \left\{g_0(\rho)\ln(\Omega + q) + [1 - g_0(\rho)]\ln(\Omega + 1)\right\}, \quad (5)$$

where, without loss of generality, we have assumed that $\varepsilon_{weak} = 0$ and consequently defined $q \equiv \exp(\varepsilon_{HB}/k_BT)$.

C. Results

Values for the model parameters are listed in Table I. Those for the hydrogen-bonding part are taken following the original work of Poole *et al.*, with identical values for ε_{HB} and Ω and our own choice for ρ_{HB} and σ.[24] Furthermore, a and b were fixed so as to provide a reasonable overall description of densities, response functions, and location of the liquid-gas and liquid-liquid critical points, the coordinates of the latter being listed in Table II. The value of the water molecule diameter, obtained from b, is 2.9 Å, a rather reasonable number.

Appendix A contains explicit expressions for the thermodynamic properties including response functions and conditions of criticality. Liquid-liquid binodals have been computed by equating the temperature, pressure, and chemical potential of the coexisting phases [see Eqs. (A2) and (A3)]. On the other hand, on solving (A6) and (A7) for ρ and T and, then, (A3) for p, the critical-point coordinates have been obtained (see Table II). Figure 1 shows the relevant portion of the liquid-liquid phase diagram in the T–ρ and p–T planes. As can be seen, the coexistence curve in the pressure-temperature plane is characterized by a negative slope. According to Clausius-Clapeyron relation, $(dp/dT)_{coex}/\rho'\rho'' = -\Delta S/\Delta\rho$, a negatively sloped coexistence curve reflects that the ordered phase is that with the lower density. Figure 1(b) also shows the so-called

TABLE I. Poole *et al.* model parameter values for the pure fluid. a is in J m^{-3} mol^{-2}; b in cm^3 mol^{-1}; ρ_{HB} and σ in mol cm^{-3}; and ϵ_{HB} in J mol^{-1}.

a	b	ρ_{HB}	σ	Ω	ε_{HB}
0.4	7.5	0.05	0.01	50 237	22 000

TABLE II. Coordinates of critical points for Poole *et al.* model.

	T_c (K)	p_c (bar)	ρ_c (g cm^{-3})
Liquid-gas	605.07	314	0.313
Liquid-liquid	266.51	2120	1.110

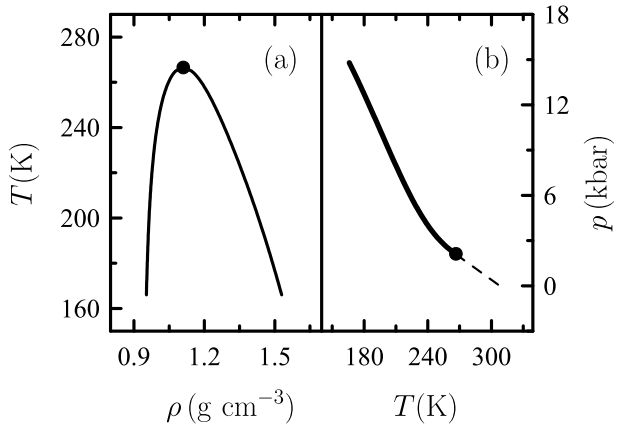

FIG. 1. Liquid-liquid coexistence in the temperature-density plane (a) and the pressure-temperature plane [bold line in (b)] for Poole *et al.* model with the parameters of Table I. The thin dashed line in (b) is the Widom line.

Widom line, regarded a continuation of the coexistence curve to the one-phase region. This single locus corresponds to maxima of the correlation length close to criticality and, as a consequence, of extrema for all thermodynamic response functions. As Fig. 1(b) shows, it extends to higher temperatures and lower pressures for Poole *et al.* model.

Figure 2 displays the density and response functions as a function of temperature at $p = 1$ bar. To calculate them, Eq. (A3) was first solved for ρ at each prescribed T. Then, with pairs of values for these two state variables, response functions were straightforwardly obtained from (A11) to (A15).

As can be seen in Fig. 2, the model qualitatively reproduces the basic features of water anomalous thermodynamics, from the density maximum at near-room temperatures to extrema of thermodynamic response functions at lower temperatures. The locus of density maxima in the pressure-temperature plane has a negative slope: $T_{MD} \approx 303$ K at

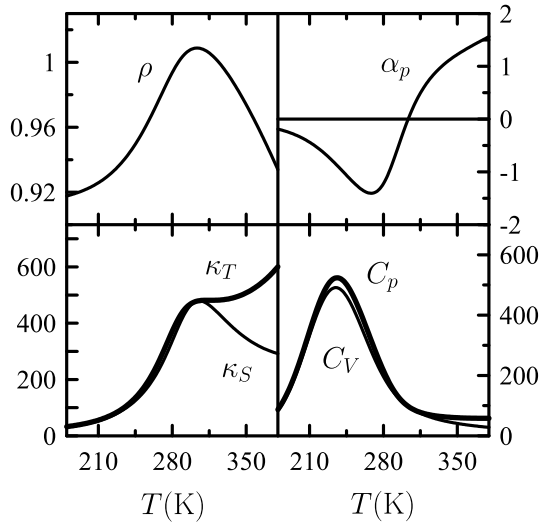

FIG. 2. Poole *et al.* model values as a function of temperature T at $p = 1$ bar for the density ρ (in g cm^{-3}), isobaric thermal expansivity α_P (in kK^{-1}), isothermal compressibility κ_T (in TPa^{-1}), isentropic compressibility κ_S (in TPa^{-1}), isobaric heat capacity C_P (in J K^{-1} mol^{-1}), and isochoric heat capacity C_V (in J K^{-1} mol^{-1}).

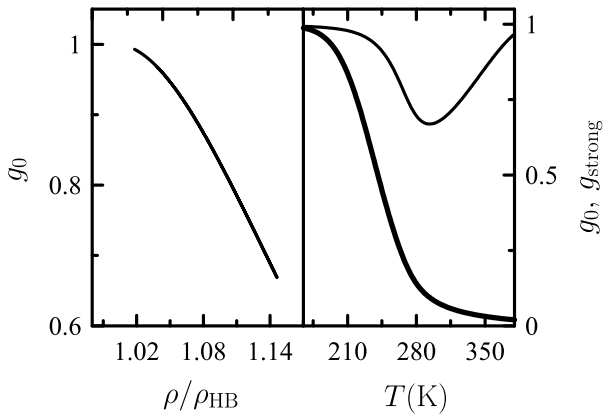

FIG. 3. Poole *et al.* model values for the fraction of A-type bonds g_0 as a function of density ρ and temperature T (thin line) at $p = 1$ bar; the bold line corresponds to the fraction of strong hydrogen bonds g_{strong}.

$p = 1$ bar, $T_{\text{MD}} \approx 299$ K at $p = 1000$ bars, and $T_{\text{MD}} \approx 278$ K at $p = 2000$ bars. It follows from thermodynamic arguments[25] that κ_T increases as temperature decreases along an isobar and in the vicinity of the T_{MD} locus. On the other hand, heat capacity maxima arise as they do for any two-energy-level system. In summary, as noted originally,[5] a reasonable picture emerges on adding the basic microscopic features of hydrogen bonding in low-temperature water to a van der Waals-like term.

One may further note that only a portion of the Gaussian representing $g_0(\rho)$ is covered for temperatures between 180 K and 380 K. Such region, plotted in Fig. 3, corresponds to densities higher than the optimal one, $\rho_{\text{HB}} \approx 0.908$ g cm^{-3}. More specifically, as Fig. 3 illustrates, from high to low temperatures, g_0 first decreases along the right branch of the Gaussian until the temperature of maximum density is reached. Then, g_0 increases with further temperature decrease. Figure 3 also shows the fraction of strong hydrogen bonds, $g_{\text{strong}} \equiv qg_0/(\Omega + q)$, as a function of temperature.

III. EXTENDED MODEL

A. Dilute solutions of nonelectrolytes

Upon the addition of solute (species 2), the one-fluid approximation straightforwardly yields the van der Waals-like part of the model in (1),

$$f_{\text{vdW}} = k_BT\left\{\sum_{i=1}^{2}\rho_i \ln[\rho_i\Lambda_i^3(T)] + \rho[h_1(y) - 1]\right\} - a\rho^2, \quad (6)$$

where $\rho_i \equiv N_i/V$ serves to denote the number densities of solvent ($i = 1$) and solute ($i = 2$), $\rho = \rho_1 + \rho_2$ while, as usual,[26]

$$a = \frac{1}{\rho^2}\sum_{i=1}^{2}\sum_{j=1}^{2}a_{ij}\rho_i\rho_j, \quad b = \frac{1}{\rho^2}\sum_{i=1}^{2}\sum_{j=1}^{2}b_{ij}\rho_i\rho_j, \quad (7)$$

with

$$a_{12} = (a_{11}a_{22})^{\frac{1}{2}}, \quad b_{12} = \frac{1}{2}(b_{11} + b_{22}). \quad (8)$$

We will scale a_{ij} and b_{ij} by a_{11} and b_{11} so that the three following dimensionless quantities will appear henceforth:

$$A_{12} \equiv \frac{a_{12}}{a_{11}}, \quad B_{22} \equiv \frac{b_{22}}{b_{11}}, \quad t \equiv k_BT\frac{b_{11}}{a_{11}}. \quad (9)$$

As for f_{HB}, since now there are $2N\rho_1/\rho$ bonds, the natural variable for g_0 is ρ_1. Hence we adopt

$$f_{\text{HB}} = -2\rho_1k_BT \times\{g_0(\rho_1)\ln(\Omega + q) + [1 - g_0(\rho_1)]\ln(\Omega + 1)\}, \quad (10)$$

with the parameters ε_{HB}, Ω, ρ_{HB}, and σ kept fixed to their pure-fluid values.

We restrict ourselves to small enough concentration of solute in solvent so that ideal-dilute solution laws (i.e., Henry's law, van't Hoff's law, etc.) are obeyed. With this proviso, our major assumption, implicit in the simple form of Eq. (10), is that no structural effects induced by solute molecules in neighboring waters[13,14] are considered. Expressions for the thermodynamic properties of such an extended Poole *et al.* model are given in Appendix B.

B. Critical loci

Critical lines can be calculated algebraically by means of a method introduced by Tisza[27] in which, by an appropriate Legendre transform, $f(T, \rho_1, \rho_2)$ is converted to a free energy that depends solely on one density variable, e.g., $f(T, \mu_1, \rho_2)$. Alternatively, one may solve the equations that, according to thermodynamic stability criteria, define the critical line in terms of second and third derivatives of $f(T, \rho_1, \rho_2)$,[28]

$$f_{\rho_1\rho_1} - f_{\rho_2\rho_2} = 0, \quad (11)$$

$$f_{\rho_1\rho_1\rho_1}f_{\rho_2\rho_2}^2 - f_{\rho_2\rho_2\rho_2}f_{\rho_1\rho_1}f_{\rho_1\rho_2} - 3f_{\rho_1\rho_1\rho_2}f_{\rho_2\rho_2}f_{\rho_1\rho_2} + 3f_{\rho_1\rho_2\rho_2}f_{\rho_1\rho_1}f_{\rho_2\rho_2} = 0, \quad (12)$$

where $f_{\rho_i\rho_j} \equiv (\partial^2 f/\partial\rho_i\partial\rho_j)_T$.

With explicit expressions for all those derivatives listed in Appendix B, we fixed the mole fraction of solute in solution ρ_2/ρ and solved numerically Eqs. (11) and (12) for T and ρ_1. From the resulting $T_c(\rho_2/\rho)$ and $\rho_{1,c}(\rho_2/\rho)$, the corresponding critical pressure $p_c(\rho_2/\rho)$ is determined by solving (B4).

Since we are restricted to small concentration of solute, calculations for ρ_2/ρ were carried out only up to 0.001. Figure 4(a) shows loci for a number of solutes of varying size and fixed $A_{12} = 1$. On increasing the solute-solvent molecular size ratio B_{22}, the orientation of the critical locus moves clockwise so that the liquid-liquid critical point moves towards higher temperatures and lower pressures for large enough B_{22}. As can be observed in Fig. 4(b), loci corresponding to a fixed and relatively large value of B_{22} extend towards higher temperatures and lower pressures with respect to the pure water liquid-liquid critical point, with a mild clockwise shift as A_{12} is increased.

These and further results (not shown here) lead us to conclude, in the framework of the model, that critical loci evolve towards higher temperatures and lower pressures when a solute with a molecular size sufficiently larger than that of water is added. Good candidates for experimental testing

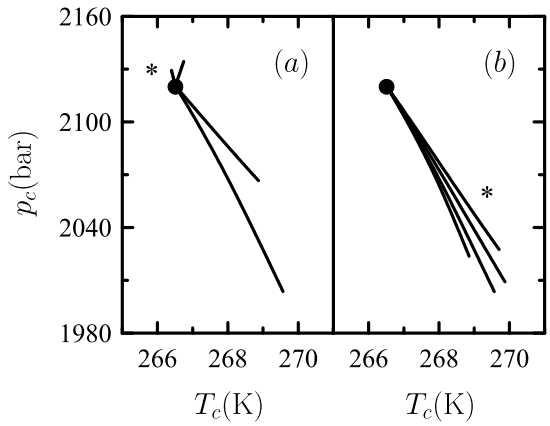

FIG. 4. Extended Poole *et al.* model values for critical loci in the pressure-temperature plane for solutes with (a) $A_{12} = 1$ and varying solute's molecular size and (b) $B_{22} = 3$ and varying strength of solute-solvent attractive interactions. In clockwise sequence, loci in (a) and (b) correspond, respectively, to $B_{22} = 0.5, 1, 2, 3$ and $A_{12} = 0.5, 1, 2, 3$; the asterisk is close to the line with $B_{22} = 0.5$ in (a) and with $A_{12} = 0.5$ in (b). As indicated in the text, all plotted lines correspond to solute mole fractions ρ_2/ρ up to 0.001.

that fulfill such condition are moderately large amphiphilic molecules. Aqueous solutions of polyols or sugars have been studied recently in this context by Murata and Tanaka.[8]

IV. HYDRATION, ATTRACTION, AND REPULSION

A. Solvation free energy

The transfer of a solute molecule from a phase α to a phase β, with the latter being a dilute liquid solution of solute in solvent, is accompanied by changes in the thermodynamic properties of the composite system $\alpha + \beta$. To quantify those changes, the so-called solvation quantities are defined.[29,30] The crucial information is contained in the solvation quantities for the liquid solution.

Let us start with the solvation free energy, μ^*, also known as excess chemical potential. According to previously described conventions,[29,30]

$$\mu^*(T, \rho_1, \rho_2) \equiv \mu_2(T, \rho_1, \rho_2) - k_B T \ln[\rho_2 \Lambda_2^3(T)]. \quad (13)$$

Attention is focused on the infinite-dilution limit, $\rho_2 \to 0$, for which the model yields

$$\frac{\mu^*(T, \rho_1)}{k_B T} = h_1(y^\circ) + B_{22} h_2(y^\circ) - \frac{2A_{12} y^\circ}{t}, \quad (14)$$

where we have used $\mu_2 = (\partial f/\partial \rho_2)_{T,\rho_1}$, $y^\circ = b_{11}\rho_1$,[31] and B_{22}, A_{12}, and t are given by Eq. (9).

Clearly, the expression for μ^* in (14) has the mathematical structure of that for the two-component Carnahan-Starling mixture. As such, it has contributions from excluded volume (the first two hard-sphere terms in the right-hand side) as well as from solute-solvent attractive interactions (the last one). No explicit hydrogen-bond contribution appears since f_{HB} does not depend on ρ_2 [see Eq. (10)]. The specific feature in (14) that differentiates this μ^* from that for a Carnahan-Starling and any other van der Waals-like mixture lies on the nonmonotonic, anomalous temperature dependence of the density of the waterlike solvent, that is, the density maximum. This feature will prove essential in what follows.

B. Solvation at constant *V*

When the volumes of the two phases remain constant during the solvation process, the solvation entropy and energy are defined as $s_V^* \equiv s_V - 3k_B/2 + k_B \ln[\rho_2 \Lambda_2^3(T)]$ and $u_V^* \equiv u_V - 3k_B T/2$, where $s_V \equiv (\partial S/\partial N_2)_{T,V,N_1}$ and $u_V \equiv (\partial U/\partial N_2)_{T,V,N_1}$. These are directly related to μ^*-derivatives via

$$\frac{s_V^*(T, \rho_1)}{k_B} = -\frac{1}{k_B}\left(\frac{\partial \mu^*}{\partial T}\right)_{\rho_1} = -[h_1(y^\circ) + B_{22} h_2(y^\circ)], \quad (15)$$

$$\frac{u_V^*(T, \rho_1)}{k_B T} = -\frac{T}{k_B}\left(\frac{\partial [\mu^*/T]}{\partial T}\right)_{\rho_1} = -\frac{2A_{12} y^\circ}{t}, \quad (16)$$

where we have used Eq. (14). The solvation entropy reflects excluded-volume effects, certainly entropic in nature, while the solvation energy is exclusively due to attractive interactions between solute and solvent.

C. Patterns of solubility

Let us first note that the solvation free energy is related to the Ostwald absorption coefficient Σ via

$$\Sigma \equiv \left(\frac{\rho_2^{\text{solution}}}{\rho_2^{\text{gas}}}\right)_{\text{coex}} = \exp\left(\frac{-\mu^*}{k_B T}\right), \quad (17)$$

where ρ_2^{solution} and ρ_2^{gas} denote the densities of solute in both solvent-rich and dilute-gas phases in mutual equilibrium. As a result, Σ is a measure of the solubility of solute in solvent, and (17) implies that a low solubility is found when $\mu^* > 0$ whereas increased values correspond to $\mu^* < 0$. In light of the thermodynamic relation

$$\frac{\mu^*}{k_B T} = \frac{u_V^*}{k_B T} - \frac{s_V^*}{k_B} = \frac{h_p^*}{k_B T} - \frac{s_p^*}{k_B}, \quad (18)$$

a low solubility arises whenever a $u_V^* < 0$ is outweighed by a more negative $T s_V^*$ [cf. Eqs. (14)–(16)].

In other words, solubility is enhanced as long as energetic contributions in (16) dominate the entropic ones in (15). Figure 5 shows h_1, h_2 and $2y_1^\circ/t$ as crucial quantities involved in such balance. Clearly, a sufficiently large B_{22}, that is, a large enough solute molecular size with respect to that of solvent, gives rise to a large $|T s_V^*|$ that outweighs $|u_V^*|$. On the other hand, sufficiently strong solute-solvent interactions, as quantified by A_{12}, result in $|u_V^*| > |T s_V^*|$.

Since the molecular size of water is quite small while attractive interactions between water and nonpolar solutes such as noble gases or hydrocarbons are weak, $|T s_V^*|$ and $|u_V^*|$ are, respectively, large and small for hydrophobic solutions. This is consistent with the very low solubility experimentally observed.

When one considers a solution of water in a liquid hydrocarbon, the situation for solute-solvent attractive interactions remains identical while, since B_{22} is now a small parameter, $|T s_V^*|$ becomes smaller and the solubility is increased as a result.[32] This picture is consistent with

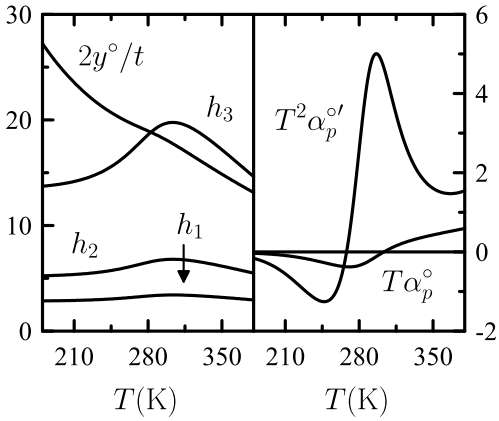

FIG. 5. Poole *et al.* model values as a function of temperature T at $p = 1$ bar for relevant quantities involved in solvation properties as described in Sections IV and V; α_p° and $\alpha_p^{\circ\prime}$ are the isobaric thermal expansivity of pure water and its temperature derivative. Values have been obtained from data plotted in Fig. 2 and expressions for h_i given in Appendix A.

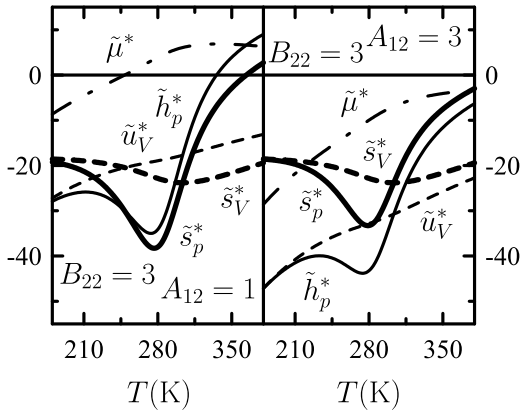

FIG. 7. Extended Poole *et al.* model values for solvation quantities as a function of temperature T at $p = 1$ bar for a hydrophobic-like solute ($B_{22} = 3$, $A_{12} = 1$) and an amphiphilic-like solute ($B_{22} = 3$, $A_{12} = 3$) in water. Dotted-dashed lines correspond to the (dimensionless) solvation free energy $\tilde{\mu}^* \equiv \mu^*/k_BT$; thin solid lines to the solvation enthalpy $\tilde{h}_p^* \equiv h_p^*/k_BT$; thin dashed lines to the solvation energy $\tilde{u}_V^* \equiv u_V^*/k_BT$; and thick lines to the constant-pressure (solid) and constant-volume (dashed) solvation entropy, $\tilde{s}_p^* \equiv s_p^*/k_B$ and $\tilde{s}_V^* \equiv s_V^*/k_B$.

experimental data (see Fig. 6 while noting that $\Sigma \propto x_2$) and confirms that the smallness of the water molecule may play a crucial role when its behavior as a solvent is concerned (see also, e.g., Ref. 34).

To further analyze the spectrum of aqueous solutions, we first focus on hard-sphere solutes (i.e., $A_{12} = 0$). This is an extreme case of hydrophobicity in which, according to Eqs. (15)–(18), solubility is very low regardless the value of the solute/solvent molecular size ratio B_{22}. On the other hand, the solubility of amphiphilic molecules like alcohols or amines in water is favored by hydrogen bonding between unlike molecules. Large A_{12} values that, according to (16), lead to $|u_V^*| > |Ts_V^*|$ serve to account for that behavior in the framework of the model.

The above features are numerically illustrated in Fig. 7, which displays μ^*, u_V^*, and Ts_V^* as a function of temperature at $p = 1$ bar for two particular choices of parameters. One of them, defined by $B_{22} = 3$ and $A_{12} = 1$, mimics hydrophobic hydration at room temperature while, with enhanced strength of solute-solvent attractive interactions, the ($B_{22} = 3$, $A_{12} = 3$) set simulates the pattern of hydration of amphiphiles.[35] All

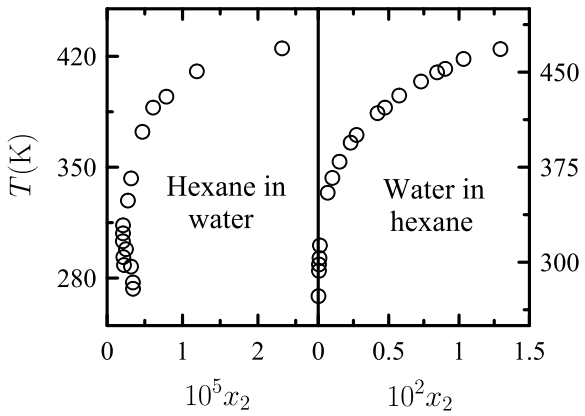

FIG. 6. Literature experimental data[33] for liquid-liquid solubility in the temperature-mole fraction (T–x_2) plane for the water-hexane system; note that x_2 denotes the mole fraction of solute.

curves were obtained on fixing T and calculating ρ_1 by solving (B4).

V. HYDRATION AND WATER ANOMALIES

A. Solvation at constant *p*

The solvation entropy s_p^* and enthalpy h_p^* associated with an isobaric process are directly related to the partial molecular entropy $s_p \equiv (\partial S/\partial N_2)_{T,p,N_1}$ and partial molecular enthalpy $h_p \equiv (\partial H/\partial N_2)_{T,p,N_1}$. Specifically, $s_p^* \equiv s_p - 3k_B/2 + k_B \ln[\rho_2\Lambda_2^3(T)]$ and $h_p^* \equiv h_p - 3k_BT/2$.

As before, these derivatives are related to μ^* but now additional factors appear,

$$\frac{s_p^*(T,\rho_1)}{k_B} = -\frac{1}{k_B}\left(\frac{\partial \mu^*}{\partial T}\right)_p + T\alpha_p^\circ = \frac{s_V^*}{k_B} + \tilde{v}_p T\alpha_p^\circ, \quad (19)$$

$$\frac{h_p^*(T,\rho_1)}{k_BT} = -\frac{T}{k_B}\left(\frac{\partial[\mu^*/T]}{\partial T}\right)_p + T\alpha_p^\circ = \frac{u_V^*}{k_BT} + \tilde{v}_p T\alpha_p^\circ, \quad (20)$$

where we have used the exact differential relation $(\partial x/\partial y)_z = (\partial x/\partial y)_w + (\partial x/\partial w)_y(\partial w/\partial y)_z$ while $\tilde{v}_p \equiv v_p/k_BT\kappa_T^\circ$, with $v_p = (\partial V/\partial N_2)_{T,p,N_1}$ the partial molecular volume and κ_T° the isothermal compressibility of the solvent; also, α_p° denotes the isobaric thermal expansivity while s_V^*/k_B and u_V^*/k_BT are given by (15) and (16). The model expression for $\tilde{v}_p$ is

$$\tilde{v}_p(T,\rho_1) - 1 = \frac{\rho}{k_BT}\left(\frac{\partial \mu^*}{\partial \rho_1}\right)_T = h_2(y^\circ) + B_{22}h_3(y^\circ) - \frac{2A_{12}y^\circ}{t}, \quad (21)$$

where, again, (14) has been used and h_3 is given in Appendix A.

A straightforward result from (19) and (20) concerns what is referred to as "enthalpy-entropy" compensation, namely, the numerical near-cancellation of the temperature derivatives of s_p^* and h_p^*/T which, according to (18), yields a near-constant μ^*/T. Because of the common $\tilde{v}_p T\alpha_p^\circ$ term in (19) and (20),

this feature relies on s_V^* and u_V^*/T. And, in accord with experiments,[36] Fig. 7 shows that our hydrophobic-like solute displays enthalpy-entropy compensation.

Further inspection of (19)–(21) reveals that the effects of intermolecular attraction and repulsion but also, via α_p°, of water anomalous thermodynamics are at play in s_p^* and h_p^*. To understand the specific consequences of this for the solubility, we first analyze the behavior of $\tilde{v}_p$.

B. Partial molecular volume

Equation (21) indicates that a competition between hard-sphere terms and solute-solvent attraction also manifests itself in the behavior of the partial molecular volume. Thus, excluded-volume effects contribute positively to $\tilde{v}_p$ while the opposite is true for intermolecular attraction. The former contribution tends to dominate since B_{22}, which is typically large, multiplies h_3, which takes on values similar to $2y^\circ/t$ (see Fig. 5). For very small B_{22} and very large A_{12}, the model supports a negative $\tilde{v}_p$.

Since the h_i functions characterizing the hard-sphere terms are monotonic in y° —and therefore the solvent's density— they all display a maximum at the $T_{\rm MD}$ (see Fig. 5). To the extent that hard-sphere contributions in (21) dominate, a $\tilde{v}_p$ vs T maximum is expected. Figure 8(a) shows that this is the case for our hydrophobic and amphiphilic-like solutes. Remarkably, experimental data for hydrocarbons and alcohols in water plotted in Fig. 8(b) constitute an experimental realization of such behavior.

C. Solubility minimum

As noted above, both (19) and (20) differ from (15) and (16) by $\tilde{v}_p T\alpha_p^\circ$. Thus the analysis of Section IV C for constant-V solvation is straightforwardly translated to constant-p solvation: a low solubility arises whenever a negative h_p^* is outweighed by a more negative Ts_p^*, etc. However, the $\tilde{v}_p T\alpha_p^\circ$ extra term makes a great difference when the temperature dependence of solvation quantities is concerned: see Fig. 7 where, in addition to $s_V^*(T)$ and $u_V^*(T)$, $s_p^*(T)$ and $h_p^*(T)$ are displayed.

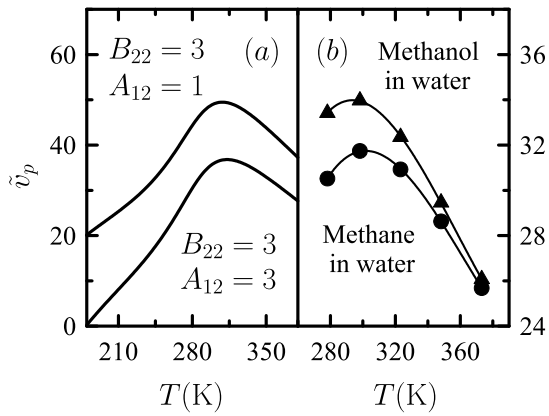

FIG. 8. Dimensionless ratio $\tilde{v}_P \equiv v_P/k_B T\kappa_T^\circ$ as a function of temperature T at $p = 1$ bar. (a) Model values for a hydrophobic-like solute ($B_{22} = 3$, $A_{12} = 1$) and an amphiphilic-like solute ($B_{22} = 3$, $A_{12} = 3$) in water. (b) Experimental data[37] for methane in water and methanol in water.

It is important to note that, beyond being very low, the solubility of hydrophobes is characterized by a minimum as a function of temperature (see Fig. 6 for hexane in water). To analyze this we combine (17), (18), and (20) to get

$$T\Big(\frac{\partial \ln \Sigma}{\partial T}\Big)_p = \frac{u_V^*}{k_B T} + (\tilde{v}_p - 1)T\alpha_p^\circ. \tag{22}$$

Now, since $u_V^*(T) < 0$ [recall (16)] while, typically, $\tilde{v}_p > 1$ (see Fig. 8), Eq. (22) establishes that a $\Sigma(T)$ minimum requires $\alpha_p^\circ(T)$ changing sign from negative to positive values as temperature is increased. Therefore, the solvent's density maximum appears essential for the solubility minimum to occur. But such condition is not sufficient since the $\Sigma(T)$ minimum can be prevented by a large $|u_V^*|$. As a matter of fact, no $\Sigma(T)$ minimum has been observed for aqueous solutions of alcohols or amines, characterized by $|u_V^*|$ values that are large in magnitude. This situation is illustrated in Fig. 7 for our model amphiphile.

We thus see that the solubility minimum is closely related to the density maximum, and it is observable whenever solute-solvent attraction is weak enough, as it is the case of pure hydrophobes. Indeed, it is evident from Eq. (22) that the temperature of the solubility minimum for a hard-sphere solute is the $T_{\rm MD}$.

The clear manifestation of the close relation between hydrophobicity and water anomalous thermodynamics was pointed out previously.[15–17] It can be rationalized at a molecular level as a natural consequence of an increase in tetrahedrality as temperature is lowered. Indeed, the local low-density states that characterize tetrahedral order favor the accommodation of solute molecules.

D. Enthalpy and entropy convergence

One infers from Eq. (20), with u_V^* given by (16), that $h_p^* = -2A_{12}y^\circ/t$ at $T_H^* = T_{\rm MD}$. This implies that the solvation enthalpy does not depend on solute's molecular size for $T = T_H^*$. Such phenomenon is known as enthalpy convergence and it is illustrated in Fig. 9.

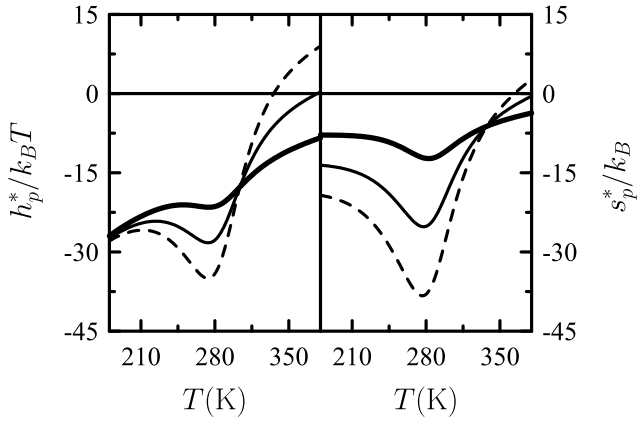

FIG. 9. Model values for the dimensionless solvation enthalpy $h_p^*/k_B T$ and entropy s_p^*/k_B as a function of temperature T at $p = 1$ bar for $A_{12} = 1$ solutes with $B_{22} = 1$ (bold solid line), $B_{22} = 2$ (thin solid line), and $B_{22} = 3$ (dashed line). Enthalpy and entropy convergence are observed at $T_H^* = T_{\rm MD} \approx 303$ K and $T_S^* \approx 338$ K, respectively. Data have been calculated as usual.

Enthalpy convergence has an entropic counterpart, entropy convergence, that is also accounted for in our model. Specifically, Eq. (19) can be conveniently rewritten in the following way:

$$\frac{s_p^*}{k_B} = \Big[1 + h_2(y^\circ) - \frac{2A_{12}y^\circ}{t}\Big]T\alpha_p^\circ - h_1(y^\circ) + [h_3(y^\circ)T\alpha_p^\circ - h_2(y^\circ)]B_{22}, \tag{23}$$

from which one infers the existence of an "entropy convergence temperature" $T_S^* > T_{\mathrm{MD}}$ at which $\alpha_p^\circ > 0$ and sufficiently high in magnitude so that $h_3(y^\circ)T\alpha_p^\circ - h_2(y^\circ) = 0$ (see Fig. 5). Also at that temperature $h_2(y^\circ)T\alpha_p^\circ - h_1(y^\circ) = 0$ in Eq. (23),[22] so $s_p^*(T_S^*)/k_B = 1 - 2A_{12}y^\circ(T_S^*)/t(T_S^*)$. Figure 9 shows three $s_p^*(T)$ curves that, as indicated, lead to $T_S^* \approx 338$ K.

In accord with previous findings,[16,17] the density anomaly, with α_p° passing from negative to positive values as temperature is increased, appears as the only factor for these convergence phenomena. Indeed, in contrast to the situation found in Sec. V C for the solubility minimum, the magnitude of solute-solvent attractive interactions is irrelevant. Furthermore, the present results agree with some well-established experimental observations.[11] Specifically, $T_S^* > T_H^*$, $s_p^*(T_S^*)$ is small in magnitude for hydrophobic solutes, and a variety of solutes in water, including pure hydrophobes and amphiphiles, exhibit both enthalpy and entropy convergence.

The $h_p^*(T)$ and $s_p^*(T)$ low-temperature minima in Fig. 9 are consistent with what Paschek[38] found from simulations for a Lennard-Jones solute in TIP5P-E water in the supercooled regime. This behavior certainly reflects the α_p° minimum in Fig. 2, which may be substantially overestimated, however, in our model (see Ref. 7 for experimental data).

E. Partial molecular heat capacities

For the partial molecular isochoric heat capacity, one gets

$$\tilde{C}_V \equiv \frac{T}{k_B}\Big(\frac{\partial s_V}{\partial T}\Big)_V = \frac{3}{2} - T\Big(\frac{\partial^2\mu^*}{\partial T^2}\Big)_{\rho_1} = \frac{3}{2}, \tag{24}$$

where we have used (15). The constant $\tilde{C}_V$ thus found stems from the simple nature of the model, which goes back to the original work of van der Waals.

We shall see next that, as found for the partial molecular volume in Sec. V B, the partial molecular isobaric heat capacity $\tilde{C}_p$ embodies an interesting interplay among water anomalous thermodynamics, excluded volume, and intermolecular attraction. Also, comparison between $\tilde{C}_V$ and $\tilde{C}_p$ emphasizes that constant-V and constant-p solvation differ dramatically. Concretely, from (14) and (19) or (20), one gets

$$\begin{aligned}\tilde{C}_p &\equiv \frac{T}{k_B}\Big(\frac{\partial s_p}{\partial T}\Big)_p = \frac{1}{k_B}\Big(\frac{\partial h_p}{\partial T}\Big)_p \\ &= \frac{3}{2} - T\Big(\frac{\partial^2\mu^*}{\partial T^2}\Big)_p + 2T\alpha_p^\circ + T^2\alpha_p^{\circ\prime} \\ &= \frac{\tilde{C}_V}{k_B} + [1 + h_2(y_1) + B_{22}h_3(y_1)][2T\alpha_p^\circ + T^2\alpha_p^{\circ\prime}] \\ &\quad - [h_3(y_1) + B_{22}h_4(y_1)](T\alpha_p^\circ)^2 \\ &\quad + \frac{2A_{12}y_1}{t}[(T\alpha_p^\circ)^2 - T^2\alpha_p^{\circ\prime}],\end{aligned} \tag{25}$$

where we have used the following identity:

$$\Big(\frac{\partial^2\mu^*}{\partial T^2}\Big)_p = \Big(\frac{\partial^2\mu^*}{\partial T^2}\Big)_{\rho_1} - 2\rho_1\frac{\partial^2\mu^*}{\partial T\partial\rho_1}\alpha_p^\circ - \rho_1\Big(\frac{\partial\mu^*}{\partial\rho_1}\Big)_T\alpha_p^{\circ\prime} + \Big[\rho_1\Big(\frac{\partial\mu^*}{\partial\rho_1}\Big)_T + \rho_1^2\Big(\frac{\partial^2\mu^*}{\partial\rho_1^2}\Big)_T\Big]\alpha_p^{\circ 2}, \tag{26}$$

with $\alpha_p^{\circ\prime} \equiv (\partial\alpha_p^\circ/\partial T)_p$.

To manage Eq. (25), we note that, as Fig. 5 shows, $T^2\alpha_p^{\circ\prime}$ is substantially greater than $T\alpha_p^\circ$. Then, in practice, the second, third, and fourth terms in the right-hand side simplify to $T^2\alpha_p^{\circ\prime}\tilde{v}_p$. This means that, at high enough temperatures so that $T^2\alpha_p^{\circ\prime} > 0$, the contributions arising from hard-sphere terms and intermolecular attraction are positive and negative, respectively. Such a result is consistent with experiments showing that, at biological temperatures, hydrophobic groups in proteins contribute positively to $\tilde{C}_p$ while hydrophilic ones make negative contributions.[39]

As Fig. 10 shows for ($B_{22} = 3$, $A_{12} = 1$) and ($B_{22} = 3$, $A_{12} = 3$) model solutes, recall, characterized by $\tilde{v}_p > 0$, the temperature dependence of $\tilde{C}_p$ reflects that of $T^2\alpha_p^{\circ\prime}$ in Fig. 5(b), with no qualitative difference between pure hydrophobes and amphiphiles. Thus, as long as excluded volume dominates so that $\tilde{v}_p > 0$, $\tilde{C}_p$ is positive around room temperature, in accord with experiment.[40] But, on purely quantitative grounds, we may note that model values in Fig. 10 depart from experimental data in that the latter do not show evidence of a $\tilde{C}_p(T)$ maximum down to 273.15 K. The observation of such behavior, however, is not precluded at lower temperatures. As a matter of fact, the molecular thermodynamic theory by Ashbaugh *et al.*[16] as well as simulations involving the MB water-like model[41] shows a $\tilde{C}_p(T)$ maximum. Also consistent with these results and with the negative $\tilde{C}_p$ in Fig. 10 are Paschek simulations of a Lennard-Jones solute in TIP5P-E water: as noted originally[38] and also evident from Figs. 7 and 9, one observes that the fingerprints of hydrophobicity are lost at sufficiently low temperatures.

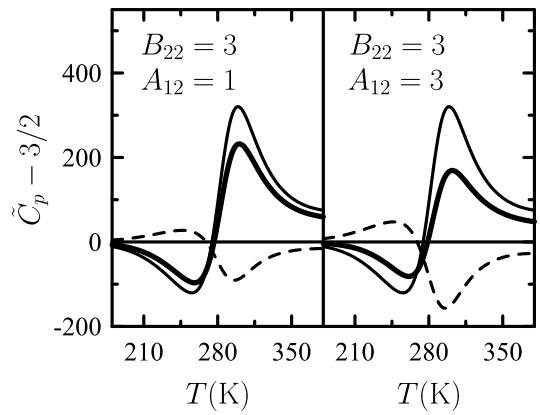

FIG. 10. Model values for the partial molecular isobaric heat capacity $\tilde{C}_p$ (bold solid line) as a function of temperature T at $p = 1$ bar for a hydrophobic-like solute ($B_{22} = 3$, $A_{12} = 1$) and an amphiphilic-like solute ($B_{22} = 3$, $A_{12} = 3$) in water. Thin solid lines correspond to the sum of the second and third terms in the right-hand side of Eq. (25) and dashed lines to the fourth one. Data have been calculated as usual.

VI. SUMMARY, DISCUSSION, AND OUTLOOK

A model free energy of water composed of van der Waals-like and hydrogen-bonding contributions is the starting point of this work. The former is constituted by a Carnahan-Starling hard-sphere term and the usual mean-field-like contribution that accounts for intermolecular attraction. The hydrogen-bonding part, originally proposed by Poole *et al.*, causes the model to mimic the anomalous thermodynamics of water at low temperatures, including the hypothesized second, liquid-liquid critical point.

The model has been generalized in Section III to describe the thermodynamic behavior of dilute solutions of small nonelectrolytes. According to standard conventions, the van der Waals-like contribution has been extended to binary mixtures while the hydrogen-bonding part remains the same. No extra assumption as to structural changes that solute molecules induce in neighboring waters has been made, and our treatment is confined to low enough solute concentrations so that contributions beyond the ideal-dilute regime can be neglected.

Within these very simple assumptions, critical lines in the pressure-temperature plane are found in Section III to develop towards experimentally accessible regions: upon the addition of a solute with a molecular size sufficiently greater than that of water, the second critical point "extends" to higher temperatures and lower pressures. This finding might be considered just a hint, in the framework of a simplified model, as to what could be expected. More concrete information is being obtained from experiments and simulations.[8] Certainly, the amount of work on aqueous solutions in connection with the second critical point has been steadily increasing during the past few years.

Section IV is devoted to the study of solvation at constant volume. In this context, it is found that the small molecular size of water, usually smaller than that of typical solutes, proves an important factor for a negative solvation entropy to outweigh the also negative solvation energy, thus giving rise to a very low solubility characteristic of hydrophobic solvation. As expected, an increase in the magnitude of solute-solvent interactions leads to an enhanced solubility that mimics the pattern of behavior of aqueous solutions of amphiphiles.

Section V deals with isobaric solvation. It is found that solvation properties differ substantially from those for the isochoric process. Our model suggests that the temperature dependence of solvation properties dramatically manifests such differences, since the density maximum plays a prominent role in isobaric solvation whereas its effect is absent for the isochoric process. We have found that many of the features regarded as signatures of hydrophobic solvation appear here as a reflection of the density anomaly. It is thus not surprising that waterlike solvation thermodynamics is found for hard spheres in a Jagla fluids that display a density maximum.[42]

In Section V C, it is shown that the solubility minimum is related to the change in sign of $\alpha_p^\circ(T)$ as temperature is increased while, in addition, the magnitude of solute-solvent attractive interactions is required to be small enough. This distinguishes pure hydrophobes, which display the solubility minimum, from amphiphiles, for which such behavior is absent. By contrast, as studied in Section V D, both enthalpy and entropy convergence occur regardless the strength of solute-solvent attraction. They are indeed a direct consequence of the density anomaly. Consistent with such model prediction is that these phenomena have been experimentally observed for a number of families of solutes of varying physicochemical nature.

The model contemplates in Section V B a $\tilde{v}_p(T)$ maximum that is also rooted in solvent's density maximum. Experimental data of $\tilde{v}_p$ for hydrocarbons and alcohols in water corroborate that result. Also in accord with experimental observations for aqueous solutions, Section V E illustrates that at near-room temperatures, excluded-volume effects and solute-solvent attractive interactions make, respectively, positive and negative contributions to the partial molecular isobaric heat capacity $\tilde{C}_p$. When the contribution from excluded volume dominates, which is the usual case, $\tilde{C}_p$ becomes negative at sufficiently low temperatures, indicating that one of the fingerprints of hydrophobicity is lost in that regime.

That the model accounts, at least qualitatively, for the most crucial features of water solvation without any appeal to solute-induced structural effects does not imply that such phenomena are absent. Certainly, solutes affect the structure of solvation shells, with these effects being remarkable for hydrophobes dissolved in water. On the other hand, we have found that a non-constant partial isochoric heat capacity $\tilde{C}_V$ demands modeling beyond what has been done here. The question then arises to what extent solute-induced structural changes in solvent contribute to $\tilde{C}_V$. Since the temperature dependence of heat capacities (isobaric and isochoric) of liquids and liquid mixtures are known to be highly sensitive to "structure" (see, e.g., Ref. 43), it is tempting to speculate that a sufficiently detailed study of $\tilde{C}_V(T)$ would prove informative.[44]

As a natural extension of the present work, it is worth mentioning the characterization of pressure effects as well as the generalization of our model to aqueous solvation of ionic species. Simulations would surely help to thoroughly characterize solvation at constant volume, and also the temperature dependence of heat capacities. Work in this direction is currently being planned.

ACKNOWLEDGMENTS

This work has benefited from stimulating discussions with B. Widom while careful reading of the manuscript by Diego González-Salgado is greatly appreciated. Research by C.A.C. has been supported by the Spanish Ministry of Economy and Competitiveness under Grant Nos. FIS2011-29614 and PR2009-0449. P.G.D. gratefully acknowledges the support of the National Science Foundation (Grant Nos. CBET-1263565 and CHE-1213343).

APPENDIX A: PROPERTIES FOR POOLE *ET AL.* MODEL

From $df = -sdT + \mu d\rho$, with f given by (1), (3), and (5), the entropy per unit volume s, chemical potential μ, and pressure p are readily obtained,

$$s = -\left(\frac{\partial f}{\partial T}\right)_{\rho} = \rho k_B \left\{\frac{5}{2} - \ln[\rho\Lambda^3(T)] - h_1(y)\right\} + 2\rho k_B \left\{g_0 \ln(\Omega + q) + [1 - g_0]\ln(\Omega + 1) - g_0 \frac{\varepsilon_{HB}}{k_B T}\frac{q}{\Omega + q}\right\}, \quad \text{(A1)}$$

$$\mu = \left(\frac{\partial f}{\partial \rho}\right)_{T} = k_B T\left\{\ln[\rho\Lambda^3(T)] + h_1(y) + h_2(y)\right\} - 2a\rho - 2k_B T\left\{g_0 \ln(\Omega + q) + [1 - g_0]\ln(\Omega + 1) + \rho g_0' \ln\left(\frac{\Omega + q}{\Omega + 1}\right)\right\}, \quad \text{(A2)}$$

$$p = \rho\mu - f = \rho k_B T[1 + h_2(y)] - a\rho^2 - 2\rho_2 k_B T g_0' \ln\left(\frac{\Omega + q}{\Omega + 1}\right), \quad \text{(A3)}$$

where

$$g_0'(\rho) = -\frac{2}{\sigma^2}(\rho - \rho_{HB})g_0(\rho), \quad \text{(A4)}$$

$$h_1(y) \equiv \frac{4y - 3y^2}{(1 - y)^2}, \quad h_2(y) \equiv \frac{4y - 2y^2}{(1 - y)^3}. \quad \text{(A5)}$$

Second and third-order derivatives yield the conditions of criticality,

$$\left(\frac{\partial^2 f}{\partial \rho^2}\right)_T = \frac{k_B T}{\rho}[1 + h_2(y) + h_3(y)] - 2a - 2k_B T \ln\left(\frac{\Omega + q}{\Omega + 1}\right)[2g_0' + \rho g_0''] = 0, \quad \text{(A6)}$$

$$\left(\frac{\partial^3 f}{\partial \rho^3}\right)_T = \frac{-k_B T}{\rho}[1 + h_3(y) - h_4(y)] - 2k_B T \ln\left(\frac{\Omega + q}{\Omega + 1}\right)[3g_0'' + \rho g_0'''] = 0, \quad \text{(A7)}$$

with

$$g_0''(\rho) = -\frac{2}{\sigma^2} g_0(\rho)\left[1 - \frac{2}{\sigma^2}(\rho - \rho_{HB})^2\right], \quad \text{(A8)}$$

$$g_0'''(\rho) = \frac{4}{\sigma^4}(\rho - \rho_{HB})g_0(\rho)\left[3 - \frac{2}{\sigma^2}(\rho - \rho_{HB})^2\right], \quad \text{(A9)}$$

$$h_3(y) \equiv \frac{4y + 4y^2 - 2y^3}{(1 - y)^4}, \quad h_4(y) \equiv \frac{4y + 20y^2 + 2y^3 - 2y^4}{(1 - y)^5}. \quad \text{(A10)}$$

The isochoric heat capacity per particle $C_V \equiv T(\partial s/\partial T)_\rho/\rho$, the isothermal compressibility $\kappa_T \equiv (\partial \ln \rho/\partial p)_T$, and the thermal pressure coefficient $(\partial p/\partial T)_V$ are

$$C_V = \frac{3}{2}k_B + 2k_B g_0\left(\frac{\varepsilon_{HB}}{k_B T}\right)\frac{\Omega q}{(\Omega + q)^2}, \quad \text{(A11)}$$

$$\kappa_T = \rho k_B T[1 + h_2(y) + h_3(y)] - 2a\rho^2 - 2\rho k_B T \ln\left[\frac{\Omega + q}{\Omega + 1}\right], \quad \text{(A12)}$$

$$\left(\frac{\partial p}{\partial T}\right)_V = \rho k_B[1 + h_2(y)] - 2k_B\rho^2 g_0'\left[\ln\left(\frac{\Omega + q}{\Omega + 1}\right) - \frac{\varepsilon_{HB}}{k_B T}\frac{q}{\Omega + q}\right], \quad \text{(A13)}$$

where we have used $(\partial\rho/\partial\mu)_T = \rho(\partial\rho/\partial p)_T$ and $(\partial p/\partial T)_V = s + \rho(\partial\mu/\partial T)_\rho$. The isobaric thermal expansivity $\alpha_p \equiv -(\partial \ln \rho/\partial T)_p$, the isobaric heat capacity per particle $C_p \equiv T(\partial s/\partial T)_p/\rho$, and the isentropic compressibility $\kappa_S \equiv (\partial \ln \rho/\partial p)_S$ then follow from

$$\alpha_p = \kappa_T\left(\frac{\partial p}{\partial T}\right)_V, C_p = C_v + \frac{T}{\rho}\alpha_p\left(\frac{\partial p}{\partial T}\right)_V, \quad \text{(A14)}$$

$$\kappa_S = \kappa_T - \frac{T\alpha_p^2}{\rho C_p}. \quad \text{(A15)}$$

APPENDIX B: PROPERTIES FOR THE EXTENDED MODEL

To obtain the entropy per unit volume, the chemical potentials, and the pressure, we start from $df = -sdT + \mu_1 d\rho_1 + \mu_2 d\rho_2$, with f given by (1), (6), and (10),

$$s = -\left(\frac{\partial f}{\partial T}\right)_{\rho_1,\rho_2} = \rho k_B\left[\frac{5}{2} - h_1(y)\right] - k_B\sum_{i=1}^{2}\rho_i \ln[\rho_i\Lambda_i^3(T)] + 2\rho_1 k_B\left\{g_0 \ln(\Omega + q) + [1 - g_0]\ln(\Omega + 1) - g_0\frac{\varepsilon_{HB}}{k_B T}\frac{q}{\Omega + q}\right\}, \quad \text{(B1)}$$

$$\mu_1 = \left(\frac{\partial f}{\partial \rho_1}\right)_{T,\rho_2} = k_B T\left\{\ln[\rho_1\Lambda_1^3(T)] + h_1(y) + h_2(y)\frac{b_{11}}{b}\right\} - 2(\rho_1 a_{11} + \rho_2 a_{12}) - 2k_B T\left\{g_0 \ln(\Omega + q) + [1 - g_0]\ln(\Omega + 1) + \rho_1 g_0' \ln\left(\frac{\Omega + q}{\Omega + 1}\right)\right\}, \quad \text{(B2)}$$

$$\mu_2 = \left(\frac{\partial f}{\partial \rho_2}\right)_{T,\rho_1} = k_B T\left\{\ln[\rho_2\Lambda_2^3(T)] + h_1(y) + h_2(y)\frac{b_{22}}{b}\right\} - 2(\rho_1 a_{12} + \rho_2 a_{22}), \quad \text{(B3)}$$

$$p = \rho_1\mu_1 + \rho_2\mu_2 - f = \rho k_B T[1 + h_2(y)] - a\rho^2 - 2\rho_1^2 k_B T g_0' \ln\left(\frac{\Omega + q}{\Omega + 1}\right). \quad \text{(B4)}$$

For second and third-order derivatives, to which Eqs. (11) and (12) are referred, the following systematic notation is adopted: $f_{\rho_i\rho_j} \equiv (\partial^2 f/\partial\rho_i\partial\rho_j)_T$, etc., with f being given by Eqs. (6)–(10). Explicit expressions are

$$f_{\rho_1\rho_1} = \frac{k_B T}{\rho_1} + k_B T\left[2\frac{4 - 2y}{(1 - y)^3}b_{11} + \rho\frac{10 - 4y}{(1 - y)^4}b_{11}^2\right] - 2a_{11} - 2k_B T \ln\left(\frac{\Omega + q}{\Omega + 1}\right)[2g_0' + \rho_1 g_0''], \quad \text{(B5)}$$

$$f_{\rho_2\rho_2} = \frac{k_B T}{\rho_2} + k_B T\left[2\frac{4 - 2y}{(1 - y)^3}b_{22} + \rho\frac{10 - 4y}{(1 - y)^4}b_{22}^2\right] - 2a_{22}, \quad \text{(B6)}$$

$$f_{\rho_1\rho_2} = k_BT\left[\frac{4-2y}{(1-y)^3}(b_{11}+b_{22}) + \rho\frac{10-4y}{(1-y)^4}b_{11}b_{22}\right] - 2a_{12}, \tag{B7}$$

$$f_{\rho_1\rho_1\rho_1} = -\frac{k_BT}{\rho_1^2} + k_BT\left[3\frac{10-4y}{(1-y)^4}b_{11}^2 + \rho\frac{36-12y}{(1-y)^5}b_{11}^3\right] - 2k_BT\ln\left(\frac{\Omega+q}{\Omega+1}\right)[3g_0'' + \rho_1 g_0'''], \tag{B8}$$

$$f_{\rho_2\rho_2\rho_2} = -\frac{k_BT}{\rho_2^2} + k_BT\left[3\frac{10-4y}{(1-y)^4}b_{22}^2 + \rho\frac{36-12y}{(1-y)^5}b_{22}^3\right], \tag{B9}$$

$$f_{\rho_1\rho_1\rho_2} = k_BT\left[\frac{10-4y}{(1-y)^4}(2b_{11}b_{22}+b_{11}^2) + \rho\frac{36-12y}{(1-y)^5}b_{11}^2b_{22}\right], \tag{B10}$$

$$f_{\rho_1\rho_2\rho_2} = k_BT\left[\frac{10-4y}{(1-y)^4}(2b_{11}b_{22}+b_{22}^2) + \rho\frac{36-12y}{(1-y)^5}b_{11}b_{22}^2\right]. \tag{B11}$$

[1]See, P. G. Debenedetti, J. Phys. Condens. Matter **15**, R1669 (2003), for review.

[2]See also, C. A. Angell, Annu. Rev. Phys. Chem. **34**, 593 (1983).

[3]See also, O. Mishima and H. E. Stanley, Nature **396**, 329 (1998).

[4]While, as far as we are aware, this hypothesis was first made by, G. M. Euliss and C. M. Sorensen, J. Chem. Phys. **80**, 4767 (1984); from experiments of dilute aqueous solutions of tert-butanol, it was firmly put forth from simulations of the ST2 molecular model of water by, P. H. Poole, F. Sciortino, U. Essmann, and H. E. Stanley, Nature **360**, 324 (1992); recent work by, J. C. Palmer, F. Martelli, Y. Liu, R. Car, A. Z. Panagiotopoulos, and P. G. Debenedetti, *ibid.* **510**, 385 (2014), provides evidence of a metastable liquid-liquid transition in the supercooled ST2 model.

[5]P. H. Poole, F. Sciortino, T. Grande, H. E. Stanley, and C. A. Angell, Phys. Rev. Lett. **73**, 1632 (1994).

[6]That temperature is ca. 231 K at atmospheric pressure.

[7]See, F. Mallamace, C. Corsaro, and H. E. Stanley, Proc. Natl. Acad. Sci. U. S. A. **110**, 4899 (2013); F. Mallamace, C. Corsaro, D. Mallamace, S. Vasi, C. Vasi, and H. E. Stanley, J. Chem. Phys. **141**, 18C504 (2014); Z. Wang, K. Ito, J. B. Leão, L. Harriger, Y. Liu, and S.-H. Chen, J. Phys. Chem. Lett. **6**, 2009 (2015); Z. Wang, A. I. Kolesnikov, K. Ito, A. Podleshyak, and S.-H. Chen, Phys. Rev. Lett. **115**, 235701 (2015), and references therein.

[8]This topic has been addressed by, S. Chatterjee and P. G. Debenedetti, J. Chem. Phys. **124**, 154503 (2006) in the context of a molecular thermodynamic theory; via experiments by, O. Mishima, *ibid.* **126**, 244507 (2007); K. Murata and H. Tanaka, Nat. Commun. **4**, 2844 (2013); Y. Suzuki and O. Mishima, J. Chem. Phys. **141**, 094505 (2014); and others; and by, D. Corradini, Z. Su, H. E. Stanley, and P. Gallo, *ibid.* **137**, 184503 (2012), see also references therein by studying model fluid mixtures with the aid of simulation techniques.

[9]N. T. Southall, K. A. Dill, and A. D. J. Haymet, J. Phys. Chem. B **106**, 521 (2002).

[10]B. Widom, P. Bhimalapuram, and K. Koga, Phys. Chem. Chem. Phys. **5**, 3085 (2003).

[11]See, F. Sedlmeier, D. Horinek, and R. R. Netz, J. Chem. Phys. **134**, 055105 (2010), and references therein for a recent account.

[12]Relevant pioneering work is, P. L. Privalov, Adv. Protein Chem. **33**, 167 (1979); R. L. Baldwin, Proc. Natl. Acad. Sci. U. S. A. **83**, 8069 (1986); B. Lee, *ibid.* **88**, 5154 (1991); N. Muller, Biopolymers **33**, 1185 (1993).

[13]H. S. Frank and M. W. Evans, J. Chem. Phys. **13**, 507 (1945).

[14]See, e.g., N. Galamba, J. Phys. Chem. B **117**, 2153 (2013); G. Graziano, *ibid.* **118**, 2598 (2014); N. Galamba, *ibid.* **118**, 2600 (2014).

[15]S. Garde, G. Hummer, A. E. García, M. E. Paulaitis, and L. R. Pratt, Phys. Rev. Lett. **77**, 4966 (1996).

[16]H. S. Ashbaugh, T. M. Truskett, and P. G. Debenedetti, J. Chem. Phys. **116**, 2907 (2002).

[17]G. Graziano and B. Lee, Biophys. Chem. **105**, 241 (2003); G. Graziano, Phys. Chem. Chem. Phys. **6**, 406 (2004); G. Graziano, J. Phys. Chem. B **109**, 12160 (2005).

[18]T. M. Truskett, P. G. Debenedetti, S. Sastry, and S. Torquato, J. Chem. Phys. **111**, 2647 (1999).

[19]N. F. Carnahan and K. E. Starling, J. Chem. Phys. **51**, 635 (1969).

[20]Note that Poole *et al.* used in Ref. 5 the original van der Waals hard-sphere term.

[21]The parameter $b = \pi d^3/6$ is associated with spherical molecules of diameter d which, in the simplest approach, is considered temperature independent.

[22]Note that $h_{i+1} = y dh_i/dy$.

[23]J. M. Prausnitz, R. N. Lichtenthaler, and E. Gomes de Azevedo, *Molecular Thermodynamics of Fluid Phase Equilibria*, 2nd ed. (Prentice Hall, New Jersey, 1986), pp. 328-333.

[24]Poole *et al.* formulated their model in Ref. 5 in terms of the volume per particle $v = 1/\rho$ so that $g_0(v) = \exp\{-[(v - v_{HB})/\sigma]^2\}$; both proposals are, obviously, equivalent.

[25]S. Sastry, P. G. Debenedetti, F. Sciortino, and H. E. Stanley, Phys. Rev. E **53**, 6144 (1996).

[26]P. H. van Konynenburg and R. L. Scott, Philos. Trans. R. Soc. London **298**, 495 (1980).

[27]See, Y. C. Kim and M. E. Fisher, J. Phys. Chem. B **105**, 11785 (2001).

[28]J. W. Tester and M. Model, *Thermodynamics and Its Applications*, 3rd ed. (Prentice Hall, New Jersey, 1997), p. 228.

[29]A. Ben-Naim, *Molecular Theory of Solutions* (Oxford University Press, New York, 2006).

[30]K. Koga, Phys. Chem. Chem. Phys. **13**, 19749 (2011); M. Ishizaki, H. Tanaka, and K. Koga, *ibid.* **13**, 2328 (2011).

[31]For convenience, henceforth we will use superscript "∘" for pure-solvent properties.

[32]This statement is true regardless the change in h_i functions that accompanies the exchanged role of water and hydrocarbon as solute and solvent.

[33]A. Macynski, B. Wisniewska-Godowska, and M. Goral, J. Phys. Chem. Ref. Data **33**, 549 (2004).

[34]M. Lucas, J. Phys. Chem. **80**, 359 (1976); B. Lee, Biopolymers **24**, 813 (1985); **31**, 993 (1991); G. Graziano, J. Chem. Soc., Faraday Trans. **94**, 3345 (1998); L. R. Pratt, Annu. Rev. Phys. Chem. **53**, 409 (2002); R. M. Lynden-Bell, N. Giovambattista, P. G. Debenedetti, T. Head-Gordon, and P. J. Rossky, Phys. Chem. Chem. Phys. **13**, 2748 (2011).

[35]D. Ben-Amotz and R. Underwood, Acc. Chem. Res. **41**, 957 (2008).

[36]See, for instance, B. Lee, Biophys. Chem. **51**, 271 (1994).

[37]G. Graziano, J. Chem. Phys. **124**, 134507 (2006).

[38]D. Paschek, Phys. Rev. Lett. **94**, 217802 (2005).

[39]N. V. Prabhu and K. A. Sharp, Annu. Rev. Phys. Chem. **56**, 521 (2005).

[40]S. J. Gill, S. F. Dec, G. Olofsson, and I. Wadsö, J. Phys. Chem. **89**, 3758 (1985).

[41]J. W. Arthur and A. D. J. Haymet, J. Chem. Phys. **110**, 5873 (1999).

[42]S. V. Buldyrev, P. Kumar, P. G. Debenedetti, P. J. Rossky, and H. E. Stanley, Proc. Natl. Acad. Sci. U. S. A. **104**, 20177 (2007); J. R. Dowdle, S. V. Buldyrev, H. E. Stanley, P. G. Debenedetti, and P. J. Rossky, J. Chem. Phys. **138**, 064506 (2013).

[43]Evident examples are near-critical states and low-temperature water. Self-association of alcohols is another case: see, e.g., C. Paz-Ramos, C. A. Cerdeiriña, and M. Costas, J. Phys. Chem. B **115**, 9626 (2011); and references therein. And aggregation of small amphiphiles is interesting in the actual context, K. Zemánková, J. Troncoso, C. A. Cerdeiriña, and L. Romaní, Chem. Phys. Lett. **640**, 184 (2015); K. Zemánková, J. Troncoso, C. A. Cerdeiriña, L. Romaní, and M. A. Anisimov, Chem. Phys. **472**, 36 (2016).

[44]The expected situation for $\tilde{C}_V$ contrasts with, e.g., the lack of sensitivity of the solubility to solute-induced structural effects pointed out by Lee (see the 1991 manuscript in Ref. 34).